Abstract

Boron nitride nanosheets prepared by an exfoliation technique were observed by aberration corrected transmission electron microscopy at 300 kV acceleration voltage. Single boron and nitrogen atoms in a monolayer region were imaged with different image contrast; a boron atom gave 16% less intensity reduction than a nitrogen atom. The number of atoms at each hexagonal ring site was determined by the image intensity that changed discretely with a 0.25 – 0.30 intensity difference. A double BN sheet was found to have a boron vacancy layer, and a triple BN layer has also a boron deficient layer on the incident surface resulting from the electron beam thinning process. The high sensitivity for atomic species was achieved by the high resolution and a small information limit due to the use of a cold field emission electron source.

Keywords: high resolution; aberration corrector; boron nitride; nanosheet

1. Introduction

The detectability of light elements by transmission electron microscopy (TEM) is enhanced as the resolution is improved, and some efforts to image a single light element atom have been recently reported. Each carbon atom in the hexagonal carbon network of a monoatomic graphene layer was resolved and imaged with high contrast by an aberration corrected microscope combined with a monochromator [1]. It was also reported that a single hydrogen atom absorbed on graphene was imaged [2].

Hexagonal boron nitride (*h*-BN) also forms a mono atomic layer (monosheet) that is very similar to graphene but the boron and nitrogen atoms are arranged alternately in the hexagonal network. Recently scanning transmission electron microscopy (STEM) with an aberration corrector resolved and identified both boron and nitrogen atoms by analysis of the annular dark field image intensity [3].

A *h*-BN monosheet has also been observed with an aberration corrected TEM with the rather low acceleration voltage of 80 kV [4,5,6] or 120 keV [7], but both atoms were imaged with the same intensity and thus they could not be discriminated from each other in the original TEM images. The intensity difference between boron and nitrogen

atoms can be detected only in the phase images retrieved by image processing [5,7].

Since the phase contrast is determined by the scattering amplitude, the intensity reduction from an incident intensity on a single light atom is proportional to the partial cross section of the atom, which depends on the atomic number of the light elements. Though the contrast is reduced by the resolution, the electron source coherency, specimen thermal oscillation and so on, boron and nitrogen atoms can be discriminated accordingly by their image intensity if an electron microscope had a sufficiently small information limit. In this paper, we report the results of observation of BN monosheet by an aberration corrected TEM.

2. Experiments

An aberration corrected TEM with a cold field emission gun (cold-FEG), R005 TEM/STEM, was used at 300 keV [8]. The aberration corrector has an asymmetric 12-pole geometry, which reduces parasite aberrations to achieve a sub-50 pm resolution [9]. The energy spread of the incident electron was estimated to be 0.6 eV from full width at half maximum of a zero loss peak in an electron energy loss

spectrum.

All images shown in this paper were recorded by a Gatan UltraScan 1000 CCD camera with using a binning 2. The original images have 1024×1024 pixels and a typical pixel size of the original images was 15 pm/pixel. All images shown in this paper was recorded with an exposure time of 1.0 sec and the signal count in a vacuum area was typically 2300 – 2400. The random noise in the TEM images was reduced by a difference filter [10] using a commercially distributed plug-in software [11], and a standard deviation of the intensity in the vacuum area was around 20 counts that is 0.8 % for the typical signal counts.

BN nanosheets were prepared by an exfoliation technique [12] in which *h*-BN particles were dispersed into a strong polar solvent, *N*,*N*-dimethylformamide (DMF) and exfoliated by ultra-sonic vibration. The peeled BN sheets were extracted by centrifugation. Drops of the DMF solution including the extracted BN nanosheets were dropped onto a Quantifoil TEM grid.

The as-synthesized BN nanosheets had thickness of several nm to 20 nm, estimated by electron energy loss spectroscopy. The BN nanosheets were thinned by

electron beam irradiation to fabricate a monosheet.

3. Results

An aberration corrected TEM image of the thinned BN nanosheet is shown in Fig. 1(a). We took a through focus series around the just focus and this image was picked up from a little under defocus condition. Third and fifth order spherical aberration coefficients when taking the image were -3.4 μm and 1.0 mm, respectively. Residual aberration coefficients measured from a tableau were listed in Table 1.

The diffractogram of the image was shown in Fig. 1(c) where some {300} reflection spots that correspond to a lattice spacing of 72 pm are observed. This suggests that a quite small information limit can be achieved by use of the cold-FEG.

In Fig. 1(a), dark dots show atomic columns forming a hexagonal ring network composed of a-sites and b-sites of *h*-BN crystal in the *p*3*m*1 (No. 14) plane group as shown in Fig. 1(d). Their minimum intensity at the columns was measured to make intensity histograms for the a-sites and the b-sites. The intensity histograms can be interpreted as combination of three Gaussian distribution functions, each of which

has a mean intensity at 0.977, 0.954 or 0.924. These values have been normalized with the intensity at the vacuum area outside of the specimen. The mean intensities decreased from unity at almost regular intervals. Since boron and nitrogen atoms have no large intensity difference, the difference in the mean intensity is due to the number of atoms contained in each site. The sites containing a single, double and triple atom are displayed, respectively, by red, yellow and green in Fig. 1(b).

In areas shown by red dashed curves in Fig. 1(b), both a-sites and b-sites consist of a single atom. We call such structure an a_1-b_1 configuration, hereafter. An area shown by a yellow dashed curve has an a_2-b_2 configuration, where both sites consist of a double atom column but an adatom is seen.

Some defect structure can be found in Fig. 1(b). Areas shown by orange dashed curves have an a_1-b_2 configuration, where the a- and b-sites consist of single atom columns (red) and double atom columns (yellow), respectively. An area shown by a green dashed curve consists of an a_2-b_3 configuration. In the present observation, thin area of *h*-BN nanosheets had mostly the a_1-b_1, a_1-b_2, and a_2-b_3 configurations, but occasionally the a_2-b_2 configuration. It is noteworthy here that the number of atoms at

the a-sites is always equal to or smaller than that at the neighbor b-sites.

Fig. 2(a) and 2(b) shows local area images extracted from square areas labeled by A and B in Fig. 1(b) where are a_1-b_1 and a_2-b_2 configurations, respectively. Though the random noises were already reduced by the difference filter in the local images, the signal to noise ratio (S/N ratio) is not enough to discriminate boron and nitrogen atoms from the original images. Some averaging process is often used to improve the S/N ratio. For example, images from between 3 and 10 exposures were averaged [4], or 20 images of a BN unit cell randomly selected from a monolayer region in an image were summed [5]. We used a following procedures to improve the S/N ratio; (1) two lattice vectors were determined from the diffractogram for the local area images, (2) the local area images were divided into several unit cells, (3) the images from all the unit cell were averaged, and furthermore (4) the image were averaged using the 2-dimensional symmetry operations of the *p*3*m*1 plane group. The results are shown in Fig. 2(c) and 2(d).

The intensity data used in the averaging process is only data in the local area images in Fig. 2(a) or 2(b). The averaging process is just valid when it can be supposed

that the structures in the local areas are uniform. The local area shown in Fig. 2(a) and 2(b) are small enough and all columns consist of the same number of atoms. It is reasonable to suppose the configuration is uniform in the local areas.

The intensity profiles along to the dashed lines are shown in Fig. 2(e) where error bars show the standard error derived from the averaging procedures. A mean values obtained from the averaging procedure is called a sample mean in statistics. The error of the sample mean can be evaluated by a standard error that is define as $s/\sqrt{N}$ where s and N are a standard deviation of the sample data and a number of data, respectively.

The intensity profiles in Fig. 2(e) show pits at the a- and b-sites, since the a- and b-sites appear as dark dots in the TEM images. The image intensity at the a-site was slightly smaller than that at the b-site in the profile for the area A with the a_1-b_1 configuration, although the difference is no more than exceeding the standard error a little. However, it may be a significant difference because it is dissimilar from that the intensity minimums at the a- and b-sites for the area B with the a_2-b_2 configuration are identical. The intensity difference suggests that single boron and nitrogen atoms can be

discriminated by the image intensity.

Here, we defined an *intensity reduction* on an atomic column by 1 - I_{min} for the minimum intensity I_{min} on the site. The a-sites were imaged with larger intensity reduction than the b-sites. Provided that the a_1 and b_1 sites are single nitrogen and boron atoms, respectively, the intensity reduction ratio $(1 - I_N)/(1 - I_B)$ is 1.16. This value is evaluated later in a section 4.2.

In the same way, local area images labeled by C and D in Fig. 1(b) are extracted in Fig. 3(a) and 3(b) where are a_1-b_2, and a_2-b_3 configurations. On the profile for a_1-b_2 configuration in Fig. 3(e), the intensity reduction at the a_1 site is similar to the a_1 site in the a_1-b_1 configuration shown in Fig. 2(e), while the intensity reduction of the b_2 site is nearly doubled. On the profile for the a_2-b_3 configuration, intensity reduction of the a_2 and b_3 sites are doubled and tripled from the profile for the a_1-b_1 configuration. The number of atoms in the columns can be measured by the intensity difference.

4. Discussion

4.1 BN layers with boron vacancies

The typical structure components in the image of the BN nanosheets in Fig. 1(a) were the a_1-b_1, a_1-b_2, a_2-b_2 and the a_2-b_3 configurations. As shown by the profiles in Fig. 2(e) and 3(e), the a-sites had smaller intensity reduction than the b-sites in the a_1-b_2, and a_2-b_3 configurations, i.e. the a-sites had the fewer number of atoms than the neighbor b-sites. Since the hexagonal BN sheets have equal number of atoms at the neighbor a- and b-sites, this implies boron or nitrogen vacancies exist on the surface. A possible structure model is shown in Fig. 4(a) where the top layer consists of a-sites vacancies shown by crosses. Here, the terraces are shown with a minimum width for simplicity but they can be expanded arbitrary.

The a_1 sites in the monolayer region were imaged with larger intensity reduction than the b_1 sites in Fig. 2(e), and thus the a_1 sites in the structure model can be assigned by single nitrogen atoms. Consequently, all sites are assigned as shown in Fig. 4(b), and the a-sites vacancies are assigned as the boron vacancies. It is consistent with the observations with the lower voltages [4,7] in which boron vacancies were often observed rather than nitrogen vacancies.

The TEM images are projected images, and thus it is unknown which surface

is an incident surface in Fig. 4. However, it has been reported that atom ejection due to electron sputtering generally occurs on the exit surface because of the large momentum transfer [13], and it has been observed that the sputtering crater forms only on the exit surface [14]. According to these pieces of evidence, it is likely that the upper boron vacancy surface and the lower stepped surface in Fig. 4(b) are the incident and exit surfaces, respectively.

4.2 Intensity reduction and partial cross section

We present a simple discussion of the partial cross section for the electron scattering in order to show that the intensity difference between boron and nitrogen atoms increases as the information limit decreases. The atomic scattering factors for boron and nitrogen listed in the literature [15] are plotted in Fig. 5(a). The factors are shown as a function of $\sin\theta/\lambda$ where λ is the incident electron wavelength. The partial cross section for electrons scattered between angles $0 \le \theta \le \alpha$ is calculated by integrating the square of the scattering factor as

$$\begin{aligned}\sigma(\alpha) &= \int_0^{\alpha} \left| f\left(\tfrac{\sin\theta}{\lambda}\right) \right|^2 2\pi \sin\theta \, d\theta \\ &\cong 2\pi\lambda^2 \int_0^{\frac{\sin\alpha}{\lambda}} |f(x)|^2 \, x \, dx.\end{aligned} \qquad \text{... (1)}$$

Here it is supposed that the scattering angle α is small and $\sin\theta/\lambda$ is replaced by x. Fig. 5(b) shows the partial cross sections for boron and nitrogen as a function of $\sin\alpha/\lambda$.

When a single atom is imaged at the optimum defocus by a TEM, the image intensity can be interpreted as a phase contrast and the intensity is evaluated as following [16],

$$I = 1 - 2\varphi_s . \qquad \text{... (2)}$$

Here φ_s is scattered wave amplitude. The scattered wave amplitude is proportional to the partial cross section $\sigma(\lambda/2L)$, where L is an information limit. Consequently, the intensity reduction 1 - $I_{\min}$ is proportional to the partial cross section.

The $\sin\alpha/\lambda$ horizontal axis in Fig. 5(b) corresponds to 1/2L. In case the information limit is larger than 0.1 nm, the partial cross sections for boron and nitrogen atoms are similar. An information limit around 70 pm is necessary to distinguish boron and nitrogen atoms by an intensity difference. The ideal intensity reduction ratio between a boron and nitrogen atoms can be estimated as 1.2 at a sufficiently small information limit, and it is comparable to the value of 1.16 obtained from the

experiment.

4.3 High resolution image simulation

High resolution images were simulated with the multi-slice method according to the structure model in Fig. 4. The simulated images for the a_1-b_1, a_2-b_2, a_1-b_2 and a_2-b_3 configurations are shown in Fig. 6(a)-(d). The spherical aberration coefficient was chosen to be -4 μm that corresponds to the measured value when taking the TEM images; the defocus was chosen to be -4.5 nm, that is an under defocus condition. The defocus spread used in the simulation was 3.4 nm in a half width at half maximum. Thermal diffuse scattering effects were neglected in the simulation.

Figs 6(e) and 6(f) show the intensity profiles for the simulated images. The simulated image can be fitted with the observed one (Fig. 2(e) and Fig. 3(e)) by using a factor of two, which is known as the Stobbs factors [17]. The following features are consistent with each other; (1) the intensity at the a_1 site that corresponds to a single nitrogen atom is slightly smaller than the one at the b_1 site that corresponds to a single boron atom, (2) the intensity at the a_2 site is larger than that at the b_2 site in both Fig.

6(f) and Fig. 3(e), though both sites correspond to a nitrogen and boron atom pair, (3) the intensities at the b_1, b_2 and b_3 sites decrease from unity at almost regular intervals, and (4) the intensities at the hexagonal ring center are larger than the incident intensity with a little pit, though the center is completely hole without any atoms.

The high resolution image intensity is affected by a defocus, aberrations and a specimen tilt. Especially, the three-fold astigmatism and the specimen tilt might make a three-fold symmetric intensity modulation. We simulated the images with the three-fold astigmatism of 38 nm or the specimen tilt of 5°, and the results were shown in a supplemental data. It was found that the intensity variance by the three-fold astigmatism of 38 nm is less than 0.001 in normalized intensity and the effects are negligible. On the other hand, the specimen tilt reduces the contrast throughout the images by 0.2 to 0.9 %, and every column images were elongated toward the azimuth of the specimen tilt. However, the columns that appear with larger intensity reduction without the sample tilt appear with larger intensity reduction even with the specimen tilt. The intensity reduction ratio never changes by the sample tilt.

The effects of the defocus on the image intensity were also evaluated and the

results were shown in the supplemental data. The structure images where every column is resolved appear at the defocus range between -7 and -1 nm. It was found from the simulation of the monolayer with the a_1-b_1 configuration that the a_1 sites show always the smaller intensity than the b_1 sites at any defocus condition. The image intensity of the both sites changes with the defocus conditions, and is minimized at a defocus of -4.5 nm. The intensity reduction ratio at the defocus condition is 1.18, a value that is consistent with both the experimental result and the ideal intensity reduction ratio discussed in the section 4.2.

The three-fold intensity modulation shown in Fig. 2 and Fig. 3 can be explained neither by the three-fold astigmatism, the specimen tilt and the defocus effects, nor their combination. The intensity modulation is due to the structure itself.

As mentioned before as the fourth feature, the intensities at the hexagonal ring center are larger than the incident intensity with a little pit. Since this feature is reappeared in the simulation, it can be interpreted as an interference effect. However, it is suspected a little that the BN sheet has a Bernal stacking structure like graphite, because it is suggested from a theoretical study that the Bernal stacked BN sheet is

stable [18]. The TEM images are simulated with the Bernal stacked structure and a stacking faulted structure model as shown in the supplemental data. The hexagonal ring center where some atoms are allocated in the model has always lower intensity than the incident intensity. Since the both structure models cannot explain the experimental results, the fourth feature can be concluded as the interference effects.

5. Conclusion

We have observed boron nitride nanosheets by aberration corrected transmission electron microscopy. The boron and nitrogen atoms in the BN nanosheets were sputtered by the high energy electron irradiation, resulting in a gradual thinning of the nanosheets. Eventually, a boron nitride monosheet appeared around the holes created by the irradiation.

The atomic columns were clearly resolved from each other and the number of atoms in the columns can be determined from the image intensity. Single boron and nitrogen atoms were also observed in the monosheet regions, and could be discriminated on the basis of intensity differences. Though the intensity difference is no

more than exceeding the standard error a little, the difference is consistent quantitatively with both the simple theoretical discussion with the partial cross section and the image simulations. This is made possible by the small enough information limit due to the use of a cold field emission electron source.

References

[1] J. C. Meyer, C. Kisielowski, R. Erni, M. D. Rossell, M. F. Crommie, A. Zettl, Nano Lett. 8 (2008) 3582.

[2] J. C. Meyer, C. O. Girit, M. F. Crommie, A. Zettl, Nature 454 (2008) 319.

[3] O. L. Krivanek, M. F. Chisholm, V. Nicolosi, T. J. Pennycook, G. J. Corbin, N. Dellby, M. F. Murfitt, C. S. Own, Z. S. Szilagyi, M. P. Oxley, S. T. Pantelides, S. J. Pennycook, Nature 464 (2010) 571.

[4] J. C. Meyer, A. Chuvilin, G. Algara-Siller, J. Biskupek, U. Kaiser, Nano Lett. 9 (2009) 2683.

[5] N. Alem, R. Erni, C. Kisielowski, M. D. Rossell, W. Gannett, A. Zettl, Phys. Rev. B 80 (2009) 155425.

[6] J. H. Warner, M. H. Rümmeli, A. Bachmatiuk, B. Büchner, ACS Nano 4 (2010) 1299.

[7] C. Jin, F. Lin, K. Suenaga, S. Iijima, Phys. Rev. Lett. 102 (2009) 195505.

[8] T. Kaneyama, T. Tomita, F. Hosokawa, H. Sawada, T. Sannomiya, S. Deguchi, M. Kawazoe, T. Miyata, E. Kobayashi, Y. Kondo, Y. Tanishiro, K. Takayanagi, Proc. IMC 16 (2006) 616.

[9] H. Sawada, Y. Tahichiro, N. Ohashi, T. Tomita, F. Hosokawa, T. Kaneyama, Y. Kondo, K. Takayanagi, J. Electron Micro. 58 (2009) 357.

[10] R. Kilaas, J. Microscopy 190 (1998) 45.

[11] The software is “HREM Filters Pro” released from HREM Research Inc.

[12] C. Zhi, Y. Bando, C. Tang, H. Kuwahara, D. Golberg, Adv. Materials 21 (2009) 1.

[13] P. A. Crozier, M. R. McCartney, D. J. Smith, Sur. Sci. 237 (1990) 232.

[14] D. Cherns, F. J. Minter, R. S. Nelson, Nucl. Instr. Methods 132 (1976) 369.

[15] C. Colliex, J. M. Cowley, et al., Electron diffraction, in: E. Prince (Ed.), International Table for Crystallography Vol. C (Third Edition), Kluwer Academic Publichers, Dordrecht, 2004, Section 4.3.

[16] J. M. Cowley, S. Iijima, Z. Naturforsch. 27A (1972) 445.

[17] M. J. Hÿtch, W. M. Stobbs, Ultramicroscopy 53 (1994) 191.

[18] L. Liu, Y. P. Feng, Z. X. Shen, Phys. Rev. B 68 (2003) 104102.

Figure Captions

Fig. 1 A TEM image of a boron nitride nanosheet (a). The atom columns are classified by the degree of intensity reduction. Red, yellow and green dots correspond to single, double and triple atom columns, respectively in (b). The associated diffractogram is shown in (c). The (300) reflection spot that corresponds to a lattice spacing of 72 pm is visible in the diffractogram. A structure model of a *h*-BN monosheet (d).

Fig. 2 Local images of a boron nitride nanosheet (a) and (b) extracted from square areas A and B in Fig. 1(a). Averaged images from the local images (c) and (d). Intensity profiles derived from the averaged images (e).

Fig. 3 Local images of a boron nitride nanosheet (a) and (b) extracted from square areas C and D in Fig. 1(a). Averaged images from the local images (c) and (d). Intensity profiles derived from the averaged images (e).

Fig. 4 A structure model of a stepped boron nitride nanosheet.

Fig. 5 Atomic scattering factors for boron and nitrogen atoms (a) [15]. Partial cross section for electron scattering by boron and nitrogen atoms (b).

Fig. 6 Simulated images of boron nitride nanosheets for an a_1-b_1 configuration (a), an a_2-b_2 configuration (b), an a_1-b_2 configuration (c), and an a_2-b_3 configuration (d). The intensity profiles derived from the simulated images (e).

Supplemental material for online publication only

Click here to download Supplemental material for online publication only: Supplement data r2.pdf

Table 1

Table 1

Aberration coefficients	Amplitude	Azimuth
Two-fold astigmatism: A_2	3.7 nm	88.9°
Axial come: P_3	78.5 nm	167.1°
Three-fold astigmatism: A_3	37.7 nm	11.0°
3rd order spherical aberration: O_4	-3.4 nm	-
Star aberration: Q_4	0.81 μm	64.7°
Four-fold astigmatism: A_4	0.29 μm	-14.5°
4th order axial coma: P_5	32.3 μm	-133.8°
Three lobe aberration: R_5	9.5 μm	-46.8°
Five-fold astigmatism: A_5	46.8 μm	21.6°
5th order spherical aberration: O_6	1.0 mm	-
Six-fold astigmatism: A_6	1.4 mm	-13.0°

Figure 1

Click here to download high resolution image

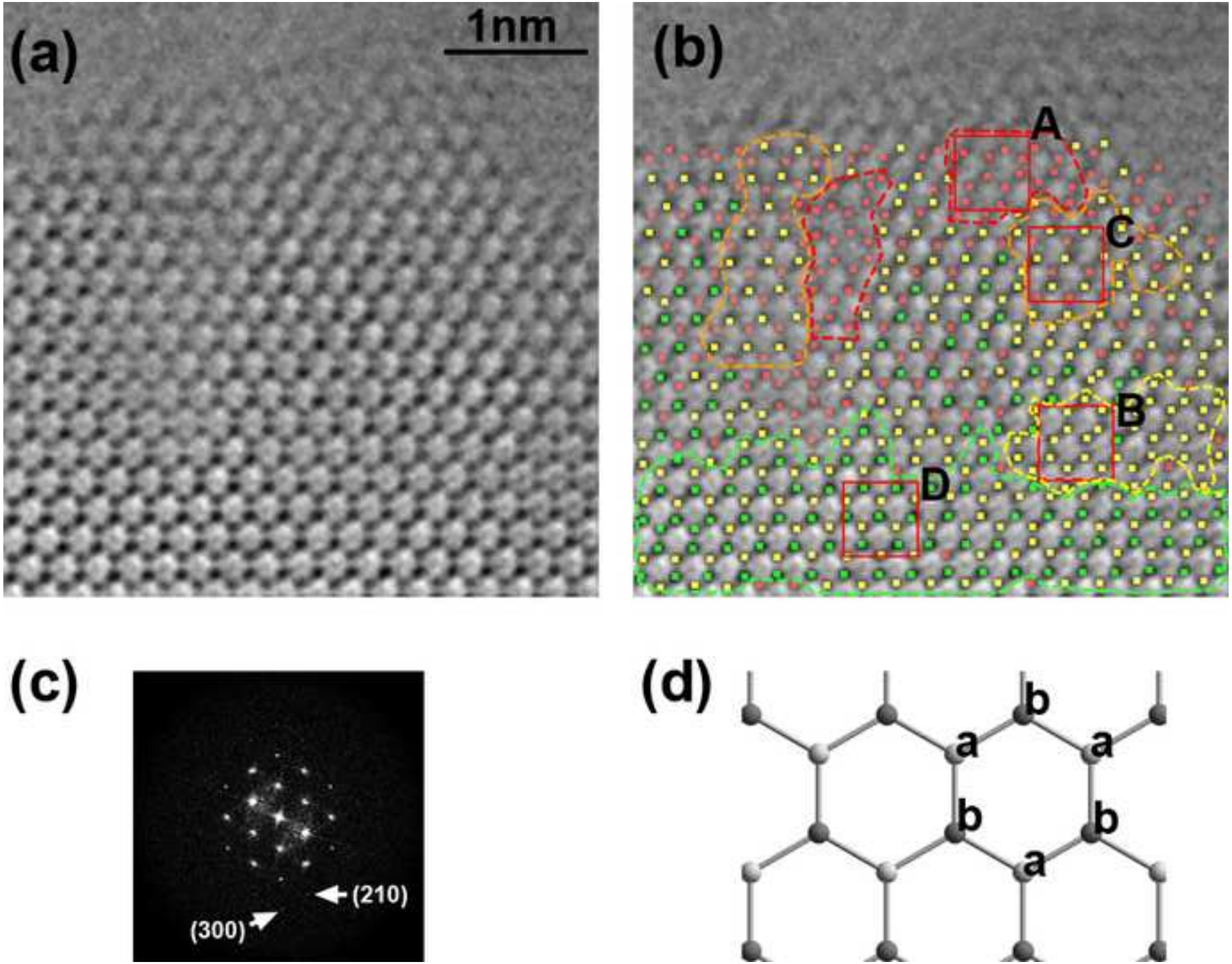

Figure 2

Click here to download high resolution image

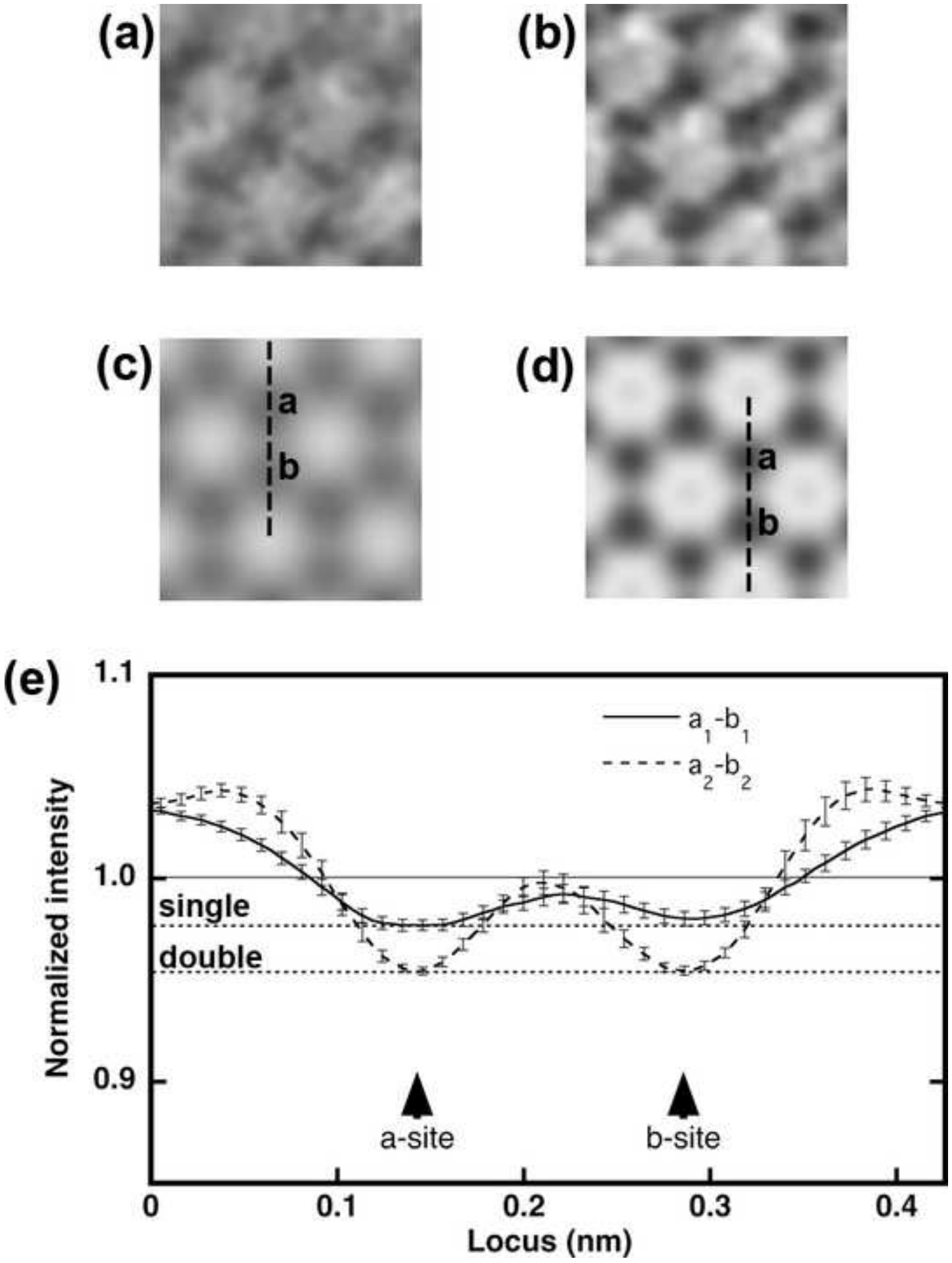

Figure 3
Click here to download high resolution image

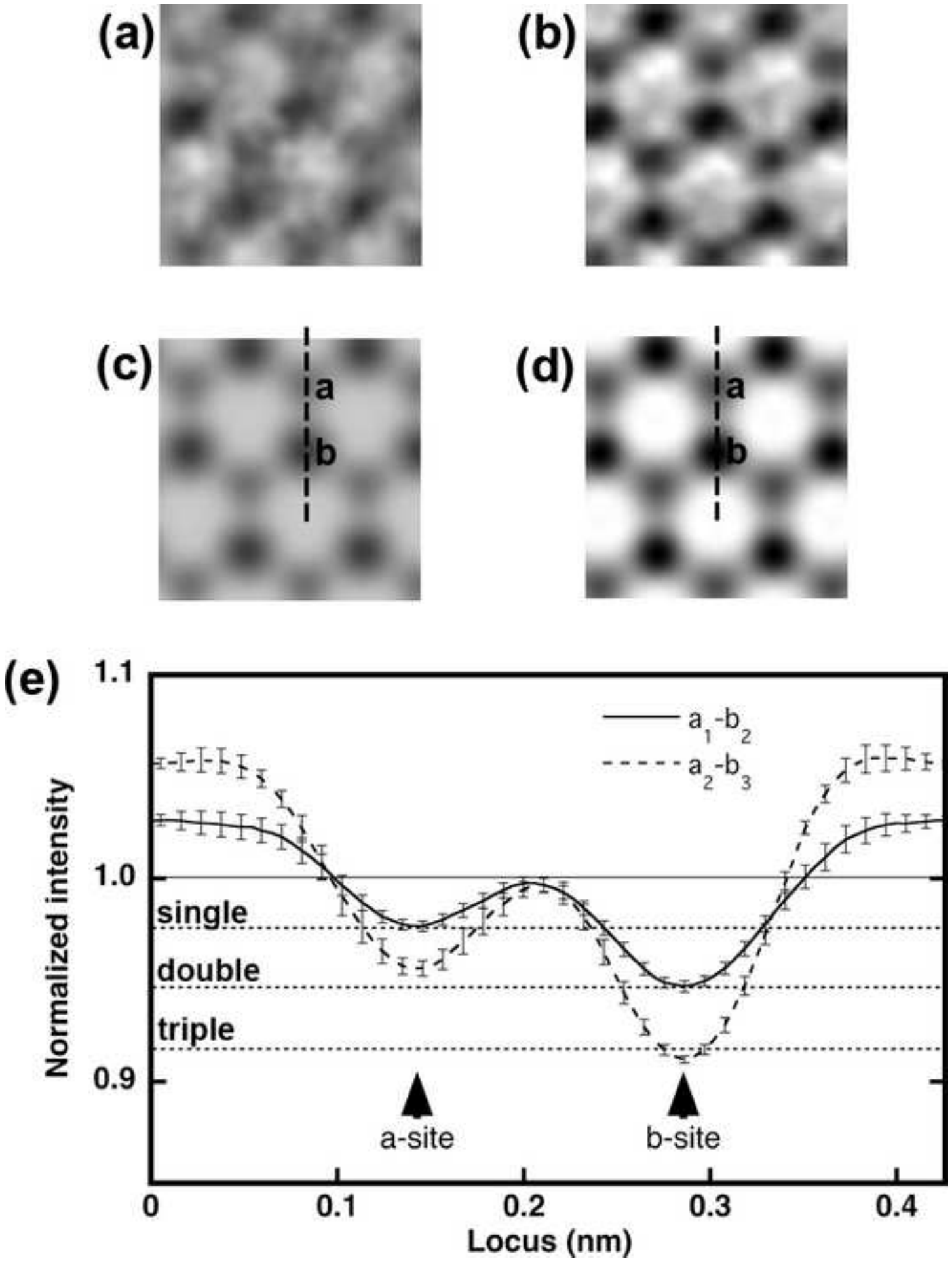

Figure 4

Click here to download high resolution image

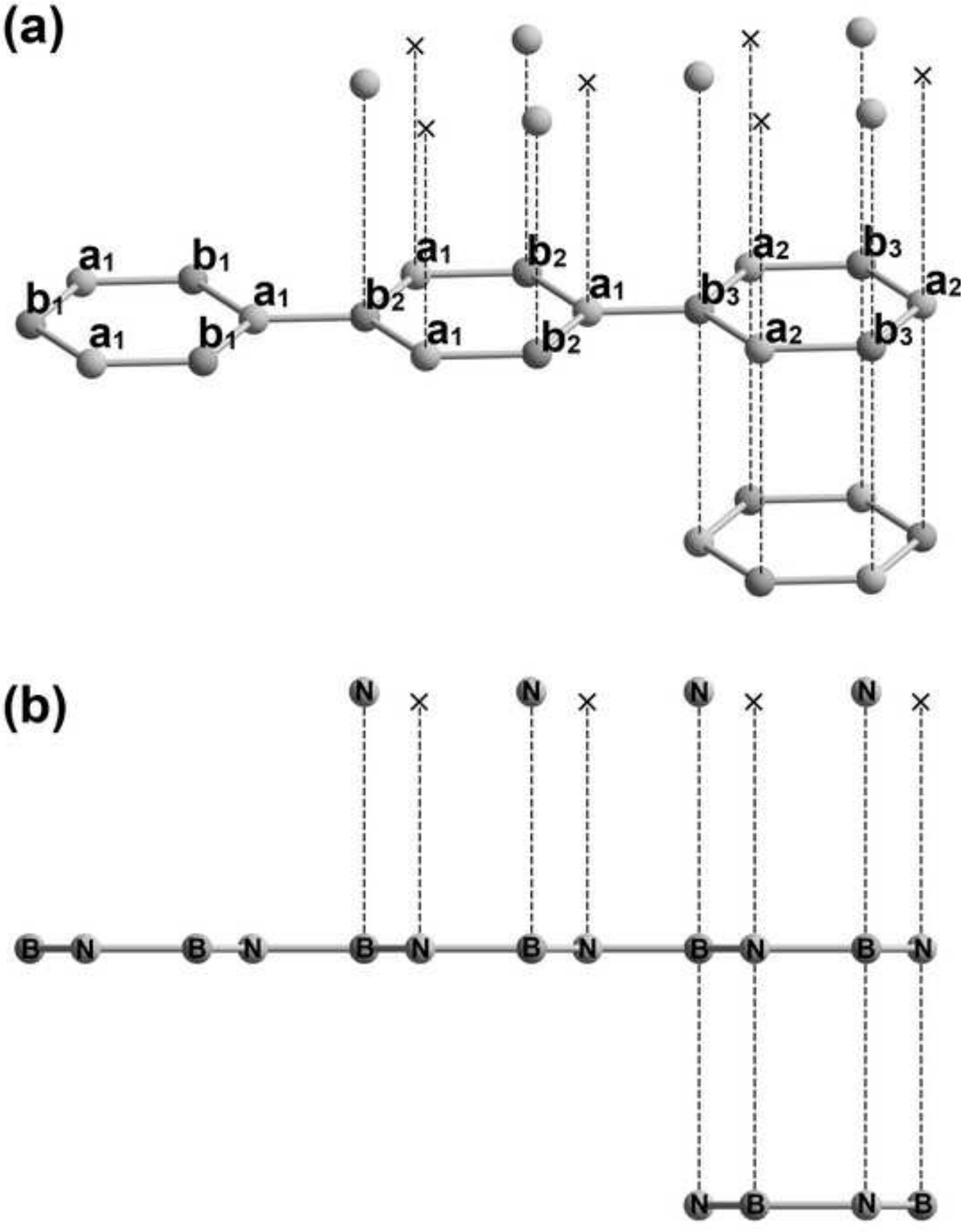

Figure 5

Click here to download high resolution image

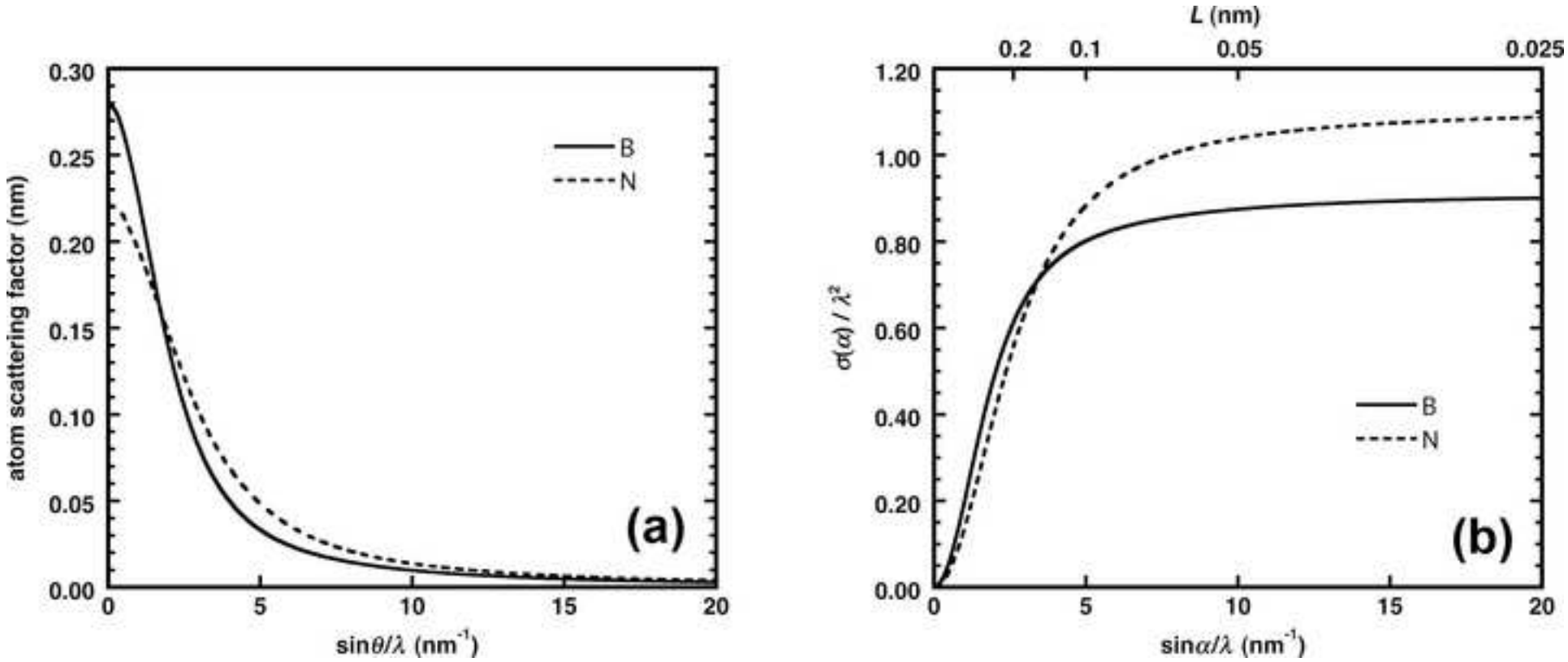

Figure 6

Click here to download high resolution image